

# Probing light mediators at ultra-low threshold energies with coherent elastic neutrino-nucleus scattering

James B. Dent<sup>a,b</sup>, Bhaskar Dutta<sup>c</sup>, Shu Liao<sup>c</sup>,

Jayden L. Newstead<sup>d</sup>, Louis E. Strigari<sup>c</sup>, and Joel W. Walker<sup>b,e</sup>

<sup>a</sup> *Department of Physics, University of Louisiana at Lafayette, Lafayette, LA 70504, USA*

<sup>b</sup> *Kavli Institute for Theoretical Physics,  
University of California, Santa Barbara, CA 93106-4030, USA*

<sup>c</sup> *Mitchell Institute for Fundamental Physics and Astronomy,  
Department of Physics and Astronomy,  
Texas A&M University, College Station, TX 77845, USA*

<sup>d</sup> *Department of Physics, Arizona State University, Tempe, AZ 85287, USA and*

<sup>e</sup> *Department of Physics, Sam Houston State University, Huntsville, TX 77341, USA*

## Abstract

Light neutral mediators, with mass  $\lesssim 1$  GeV, are common features of extensions to the Standard Model (SM). Current astrophysical and terrestrial experiments have constrained the model parameter space, and planned experiments around the world promise continued improvement in sensitivity. In this paper we study the prospects for probing light neutral mediators using terrestrial stopped pion and reactor sources in combination with ultra-low threshold nuclear and electron recoil detectors. We show that the coherent neutrino-nucleus and neutrino-electron scattering channels provide complementary sensitivity to light mediators. With low threshold detectors, we show that most stringent bounds on models arise from the nuclear scattering process, improving upon previous bounds from electron scattering of solar neutrinos by nearly an order of magnitude for mediator masses  $\gtrsim 0.1$  GeV.

## I. INTRODUCTION

Low mass particles from hidden sectors occur in many extensions of the Standard Model (SM). Examples include grand unified theories (GUTs), models that explain baryogenesis, or dark sector models that include a portal which provides a connection to SM particles. Many experiments around the world are now being developed to study light mediators and hidden sectors (see for example the review [1]).

Experiments that are designed to detect coherent elastic neutrino-nucleus scattering ( $\text{CE}\nu\text{NS}$ ) can provide a particularly important probe of light mediator models. Because the  $\text{CE}\nu\text{NS}$  process is well predicted in the SM [2], a measured deviation from it can provide a test of Beyond Standard Model (BSM) physics. These models include non-standard neutrino interactions (NSI) with new weakly coupled particles, electromagnetic properties of neutrinos, and oscillations into sterile neutrinos [3–12].  $\text{CE}\nu\text{NS}$  can also shed light onto astrophysical processes occurring in neutron stars and core-collapse supernovae [13–17].

Although experiments to measure  $\text{CE}\nu\text{NS}$  [18, 19] have been long proposed, its detection has remained elusive. However, recent experimental progress on several fronts may make detection of  $\text{CE}\nu\text{NS}$  a reality in the near future. The COHERENT experiment will use a stopped pion beam at the Spallation Neutrino Source (SNS) to detect  $\text{CE}\nu\text{NS}$  with Argon, Germanium, and CsI detectors [20], and will improve upon current NSI limits. The CONNIE experiment is currently using low-threshold CCD detectors near a GW reactor source with near term prospects for measuring the  $\text{CE}\nu\text{NS}$  process [21], and the TEXONO experiment is developing detectors to measure  $\text{CE}\nu\text{NS}$  also using a GW reactor neutrino source. These experiments will be sensitive to BSM physics such as NSI and the neutrino magnetic moment [22]. More recently, the MINER experiment at Texas A&M University has been developed to measure  $\text{CE}\nu\text{NS}$  using a MW reactor neutrino source, with sensitivity to sterile neutrinos, NSI, and the neutrino magnetic moment [10, 11].

In addition to these terrestrial efforts,  $\text{CE}\nu\text{NS}$  will also be an important aspect of direct dark matter searches. Direct detection experiments search for the interaction of dark matter (DM) with SM particles, typically via the nuclear recoil induced by elastic DM-SM scattering. As direct detection experiments continue to increase in sensitivity, the solar, atmospheric, and diffuse neutrino background from  $\text{CE}\nu\text{NS}$  will become a pressing issue. For canonical parameterizations of the DM-nucleus cross section, the presence of the  $\text{CE}\nu\text{NS}$

background will result in a situation where increasing the experimental exposure typically does not improve the sensitivity to lower cross-sections, an obstacle known as the neutrino floor [23, 24]. However, for more general parameterizations of DM interactions, the neutrino floor can be mitigated in a large fraction of the parameter space [25, 26].

Several papers have studied how  $\text{CE}\nu\text{NS}$  can be used to probe light mediators. Ref. [27, 28] use solar neutrinos at direct detection experiments, studying dark photon models and generic light mediator interactions of scalar, pseudoscalar, vector and axial-vector types. Ref. [7] analyze the sensitivity of several  $\text{CE}\nu\text{NS}$  experiments to light dark matter interacting with the SM through a light vector mediator coupled to the electromagnetic current.

In this paper we study the prospects for identifying NSI with light neutral mediators using a combination of  $\text{CE}\nu\text{NS}$  and neutrino-electron scattering experiments. New mediator particles whose masses are small compared to the typical momentum exchanged in the scattering process can significantly alter the scattering rate, with pronounced effects at low recoil kinetic energies ( $\lesssim$  keV), and are therefore an intriguing experimental target. We focus specifically on projections for the MINER experiment and the first phase of the COHERENT project, using a simplified model approach to project constraints on hidden sector models which include a new light vector boson that couples neutrinos to the lepton and quark sectors of the SM. We show that an experiment with the sensitivity of MINER can produce world-leading constraints on a  $U(1)_{\text{B-L}}$  extension of the SM. Interestingly, the most stringent bounds arise from the nuclear scattering process rather than electron scattering as in solar neutrino probes. This is because the largest solar fluxes correspond to relatively low energy regions of the neutrino spectrum, with correspondingly soft nuclear recoils below current detection thresholds, whereas reactors combine moderate neutrino energies with a large local flux. The hope for experimentally leveraging advantages of the  $\text{CE}\nu\text{NS}$  process relies upon a continued push towards lower threshold detector technologies, such as those actively being developed for direct DM searches. This program is especially central to the study of models with light mediators, given the described rate enhancement in the ultra-low recoil energy regime.

The outline of this paper is as follows. Sec. II briefly reviews some details of  $\text{CE}\nu\text{NS}$  in the SM, and Sec. III summarizes a generic simplified model extension of the SM that includes NSI via light mediators. Sec. IV describes the application of very low threshold detector technology to reactor searches. Sec. V briefly lays out the process employed for limit

setting, and Sec. VI presents our main numerical sensitivity projections, including results for a specific  $U(1)_{B-L}$  BSM model at MINER. Sec. VII examines the relative scaling of these limits in the extreme light mediator limit. In Sec. VIII, we summarize and conclude.

## II. CE $\nu$ NS IN THE STANDARD MODEL

Coherent elastic neutrino-nucleus scattering has garnered great attention as an important process for astrophysics, dark matter physics, and as a test of the Standard Model itself in a new, low energy regime. The scattering proceeds due to a neutrino of incident energy  $E_\nu$  impinging on a nuclear target, to which is imparted a kinetic recoil energy  $E_R$ . Coherent scattering arises as a pure quantum effect for incident neutrinos with small enough energy such that they are unable to probe the interior nucleon structure of the nucleus. Specifically, for momentum transfers  $|\vec{q}| \lesssim R^{-1}$ , with  $R$  the typical nuclear size, coherent scattering will generate an enhancement in the cross-section.

The differential cross-section for a neutrino scattering off of a target of mass  $m$  (such as an electron or quark) is

$$\frac{d\sigma}{dE_R} = \frac{G_F^2 m}{2\pi} \left( (g_v + g_a)^2 + (g_v - g_a)^2 \left( 1 - \frac{E_R}{E_\nu} \right)^2 + (g_a^2 - g_v^2) \frac{m E_R}{E_\nu^2} \right). \quad (1)$$

Where  $G_F$  is the Fermi constant. The vector and axial-vector couplings  $(g_v, g_a) \equiv (g_L + g_R, g_L - g_R) = (T_3 - 2Q_{\text{em}} \sin^2 \theta_W, T_3)$  are those of the scattering target with respect to the neutral current amplitude  $(T_3 - Q_{\text{em}} \sin^2 \theta_W)$  for coupling to a  $Z$ -boson, where  $T_3$  is the diagonal generator of  $SU(2)_L$ ,  $Q_{\text{em}}$  is the electromagnetic charge, and  $\theta_W$  is the weak mixing angle. Note that the neutrino's charge under the neutral current  $t$ -channel exchange has already been globally factored out in Eq. (1). In the case that the neutrino scatters off of an electron, there is an additional interference diagram for the charged-current  $t$ -channel exchange of a  $W$ -boson where the final  $(\nu_e, e^-)$  states are associated with crossed vertices. An analogous charged current interference diagram likewise exists for anti-neutrino scattering off of an electron, although it manifests instead via the  $s$ -channel. The functional form of Eq. (1) is unchanged by these additions, which may be absorbed into a simple redefinition of the scattering charges. Intuitively, the  $W$  exchange is pure left, adding a unit shift to each of  $(g_v, g_a)$ . However, if the scattering source should happen to be of the antineutrino variety, as is the case for a nuclear reactor, then the entire effective axial charge inherits a

relative negative phase, subsequent to conditional application of the positive unit shift for matched flavor. Intuitively, under  $CP$ , the inversion ( $L \Leftrightarrow R$ ) flips the sign of  $g_a$ . These transformations are summarized following.

$$[g_v, g_a] \Rightarrow [(g_v + \delta_{X,e}), \pm (g_a + \delta_{X,e})] \quad (2)$$

There is an additional complication for nuclear scattering, insomuch as one must account for the embedding of quarks into nucleons, which are in turn bound in the nucleus. This is a situation familiar from dark matter physics, with embedding prescriptions given for example in [29–32]. The vector couplings to protons and neutrons are respectively  $g_v^p = 1/2 - 2\sin^2\theta_W$  and  $g_v^n = -1/2$ . The value of  $\theta_W$  has been measured at energies of  $\sim 10\text{MeV}$  in atomic parity violation experiments [33], at energies of  $\sim 1 - 8\text{MeV}$  from reactor experiments [34], and has also been calculated in the  $\overline{\text{MS}}$  scheme at low energies [35]. In the present work we adopt the value  $\sin^2\theta_W = 0.2387$ . Given this value, one finds that the vector coupling to protons is subdominant compared to that for the neutrons. The axial couplings for protons and neutrons are respectively  $g_a^p = +1/2$  and  $g_a^n = -1/2$ , or effectively a negative of the prior for anti-neutrino scattering. The total axial coupling to nuclei is proportional to the expectation value of the nucleon spin content in the nucleus,  $\langle S_p \rangle$  and  $\langle S_n \rangle$ . These expectation values vary from element to element, with the values of interest in this work for germanium and silicon given by [36]. Since the vector coupling adds coherently while the axial charge couples (still coherently) to the differential spin of embedded nucleons, the dominant contribution to  $\text{CE}\nu\text{NS}$  will arise from vector coupling to the neutron count  $N = A - Z$ , yielding a total cross section that scales at leading order as  $N^2$ . For the case of electron scattering, we take the free electron approximation, giving rise to sharp features at the atomic energy levels.

### III. $\text{CE}\nu\text{NS}$ IN SIMPLIFIED MODEL EXTENSIONS OF THE STANDARD MODEL

We next examine modifications to the leading  $\text{CE}\nu\text{NS}$  event profile induced by the presence of new neutral current light mediators. For this analysis we will turn to a simplified model framework, which is a minimal extension of the SM that includes a new mediating particle, along with its couplings to neutrinos, electrons, and quarks. We follow a path similar to that of [28], where neutral current mediators are introduced that transform as a scalar (S), pseudoscalar (PS), vector (V), or axial-vector (AV) under the Lorentz group.

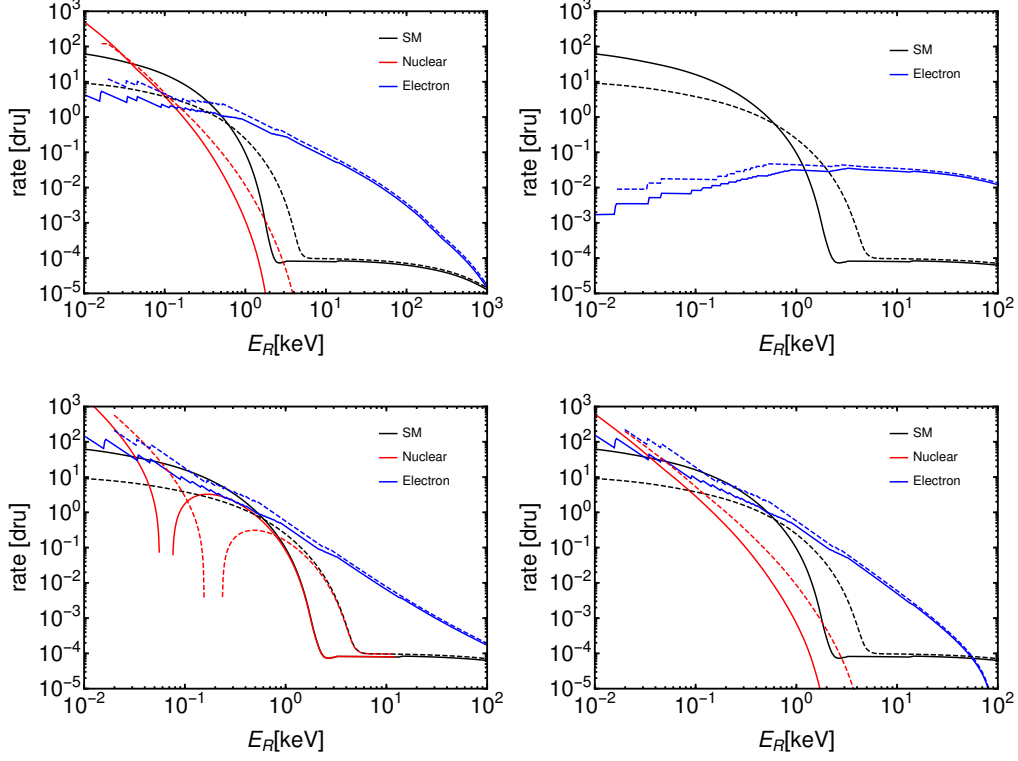


FIG. 1. Sample recoil rates for the four BSM scenarios with the following mediator types: scalar (top left), pseudoscalar (top right), vector (bottom left), or axial-vector (bottom right). The solid and dotted lines are for Ge and Si detectors respectively. The mediator mass is taken to be 1keV and the coupling chosen such that the interaction is approximately the strength of the SM.

The new interactions are specified by the following Lagrangians.

$$\mathcal{L}_S \supset \phi(g_{\nu,S}\bar{\nu}\nu + g_{\ell,S}\bar{\ell}\ell + g_{q,S}\bar{q}q) \quad (3)$$

$$\mathcal{L}_{PS} \supset \phi(g_{\nu,S}\bar{\nu}\nu - i\gamma^5(g_{\ell,PS}\bar{\ell}\ell + g_{q,PS}\bar{q}q)) \quad (4)$$

$$\mathcal{L}_V \supset Z'_\mu(g_{\nu,Z'}\bar{\nu}_L\gamma^\mu\nu_L + g_{\ell,v}\bar{\ell}\gamma^\mu\ell + g_{q,v}\bar{q}\gamma^\mu q) \quad (5)$$

$$\mathcal{L}_{AV} \supset Z'_\mu(g_{\nu,Z'}\bar{\nu}_L\gamma^\mu\nu_L - g_{\ell,v}\bar{\ell}\gamma^\mu\gamma^5\ell - g_{q,v}\bar{q}\gamma^\mu\gamma^5q) \quad (6)$$

Light mediators can be experimentally allowed, if their coupling is very weak. In place of a four-point Fermi interaction vertex, there is in this case a product of three-point couplings over a propagator explicitly dependent upon the momentum transfer  $t = -2E_R m$ . A light vector or axial vector mediator may be simply accommodated in a manner similar to the prior inclusion of charged current interference, via redefinition of the effective charges in Eq. (1). Defining the axial phase  $\alpha$  of a target species  $X$  by  $[g_{X,v}, g_{X,a}] \equiv g_{X,Z'} \times [\cos \alpha, \sin \alpha]$ , the prescription for holistic inclusion of these processes is given by the following extension of

Eq. (2).

$$[g_v, g_a] \Rightarrow [(g_v + \delta_{X,e}), \pm (g_a + \delta_{X,e})] + \frac{g_{\nu,Z'} g_{X,Z'}}{\sqrt{2}G_F (2E_R m_X + M_{Z'}^2)} \times [\cos \alpha, \pm \sin \alpha] \quad (7)$$

As before,  $(-)$  signs apply for the case of antineutrino scattering. Note that the transformation in Eq. (7) will correctly reproduce the corresponding entries in Table IV of Ref. [28] when applied to the base neutral current cross-section of Eq. (1), while also automatically generating all suppressed terms of higher order in  $E_R/E_\nu$ . For nuclear scattering, where ( $E_\nu \ll m_N$ ), we are likewise guaranteed that ( $E_R \ll E_\nu$ ) will indeed apply. On the other hand, for electron scattering, with ( $E_\nu \simeq m_e$ ), it may similarly be that  $E_R \simeq E_\nu$ . However, investigation of the factor  $2E_R m_X + M_{Z'}^2$  from the  $Z'$  propagator suggests that the region of parameter space where terms of higher order in  $E_R/E_\nu$  become relevant is typically disjoint from the region wherein the most substantial rate enhancement is derived from a light  $Z'$  mediator. Note first that the maximal kinetic recoil (for a head-on impact) impartable to a target of mass  $m_X$  is

$$E_R^{\max} = \frac{2E_\nu^2}{m_X + 2E_\nu}, \quad (8)$$

which reduces to the order of  $m_e$  for ( $E_\nu \simeq m_e$ ). In this case,  $2E_R m_e$  cannot be much greater than roughly ( $m_e^2 \approx E_\nu^2$ ), but it can be much, much smaller. This will be irrelevant if ( $M_{Z'} \gtrsim m_e$ ), such that the mediator mass-square will always dominate, generating a flat response in  $E_R$ . However, if ( $M_{Z'} \ll m_e$ ), then the event rate is substantially enhanced as  $E_R$  decreases, scaling as  $E_R^{-2}$  (taking the square of the amplitude), until leveling off for recoils much below the knee  $E_{R,e}^{\text{knee}} \equiv M_{Z'}^2/2m_e$ . In particular, note that this cutoff for the rise in the light mediator enhancement occurs, given ( $M_{Z'} \ll m_e \simeq E_\nu$ ), in a regime where  $E_R \ll E_\nu$ . No such similar statement may be made about the neglect of terms higher order in  $E_R/E_\nu$  if ( $M_{Z'} \gtrsim m_e$ ). For the nuclear case,  $E_R^{\max}$  reduces to  $2E_\nu^2/m_N$  for ( $E_\nu \ll m_N$ ). As such, the relevant upper bound is ( $2E_R m_N \leq 4E_\nu^2$ ). Correspondingly, there will be no substantial variation of the light-mediator enhancement with  $E_R$  unless ( $M_{Z'} \ll E_\nu$ ). If this is the case, then the event rate can again grow as  $E_R^{-2}$  until leveling off below an energy around  $E_{R,N}^{\text{knee}} \equiv M_{Z'}^2/2m_N$ . Note that even in the flat recoil response regime, which may onset more or less concurrently for both nuclear and electron scattering when ( $M_{Z'}^2 \gtrsim 2E_R^{\max} m_X \approx E_\nu^2$ ), it remains possible, in principle, for the BSM rate to exceed the SM rate globally if ( $M_{Z'}^2 \lesssim g_{\nu,Z'} g_{X,Z'}/G_F$ ). All of the event features described here are purely kinematic, and are broadly independent of the specific couplings or spin of the

hypothetical mediator.

There are two important bits of conventional wisdom developed in the approach to coherent nuclear scattering with heavy mediators that are now seen to be inapplicable, or at least not strictly applicable, to the case of scattering mediated by a light field. The first is that any non-standard interaction (NSI) must have cross-terms with the standard model in order to yield an appreciable rate. The usual intuition here (cf. Ref. [10]) is that NSI vertices, e.g. those representing a heavy gauge boson ( $M_{Z'} \gg M_Z$ ) with SM-comparable coupling strengths, will necessarily have amplitudes of substantially smaller magnitude than those of the SM, such that the leading new physics contribution in the square of summed amplitudes is from the interference term. A corollary of this statement is that new physics diagrams that cannot interfere with the SM, e.g. those representing flavor-changing neutral currents, will be practically invisible to experiments that are not sensitive to the final state on an event-by-event basis. For light mediators, it is quite conceivable that the failure of prior experiments to observe the corresponding signatures of new physics has been purely one of technology, namely the inability to probe very soft recoils of the target. Given a sufficient advance in technology to render the final state visible, it need not actually be weak, and a boost from interference with known SM processes is thus no longer a prerequisite to discovery. The second element of standard lore to be upended in the present context is that electron scattering is always sub-dominant to nuclear scattering in visibility at low recoil momenta. Support for this observation comes from two directions, the first being that only the nucleus is able to remain coherent for deBroglie wavelengths typical of nuclear energies, and thereby access the  $\mathcal{O}(10^2)$  relative rate enhancement associated with summing over constituents in the amplitude prior to squaring. The second advantage (or sometimes disadvantage) of nuclear scattering is purely kinematic. The cutoff scale for recoil scattering  $E_R^{\max}$  of a heavy nucleus may typically be a factor of  $10^4$  larger than the corresponding cutoff for electron recoil. Consequently, the nuclear recoil spectrum is highly concentrated inside a very narrow energy bandwidth, wherein its relative amplitude is correspondingly elevated. If the resultant recoils falls below threshold sensitivity of the detector, then they will be invisible. However, if the necessary threshold can be breached, a substantial gain in rate is attained. Whereas competing backgrounds to detection may have a very wide spectral composition, this isolation of a highly targeted integration domain is quite beneficial. Additionally, although event-by-event discrimination of nuclear from electron recoils is typically



lost in solid state detectors at very soft recoils (as the phonon vs. ionization yield curves converge or the underlying phonon signal is traded for threshold sensitivity via Luke gain, cf. CDMSlite [37]) a reasonable amount of population discrimination may be recovered simply from this radical disparity of profiles.

In the regime ( $M_{Z'}^2 \ll E_\nu^2$ ), with typical MeV scale solar or reactor neutrino energies, both the electron and nuclear  $Z'$  scattering amplitudes will grow as  $1/E_R$  with decreasing recoil energy, until flattening out at ( $E_{R,X}^{\text{knee}} \simeq M_{Z'}^2/2m_X$ ). In particular, the electron recoils will both onset ( $E_{R,e}^{\text{max}}/E_{R,N}^{\text{max}} \simeq 10^4$ ), and level off ( $E_{R,e}^{\text{knee}}/E_{R,N}^{\text{knee}} \simeq 10^5$ ), at much larger recoils for the same  $M_{Z'}$ . With identical couplings  $g_{X,Z'}$ , the single electron scattering to nuclear scattering (per particle constituent) amplitude ratio will grow linearly with increasing  $E_R$ , from parity below  $E_{R,N}^{\text{knee}}$ , up to a ceiling around  $10^5$  above  $E_{R,e}^{\text{knee}}$ . This advantage can, in principle, be more than sufficient to overcome the coherency advantage of the nucleus. However, the extended slow decline of the electron scattering rate across regions of the recoil parameter space well above several keV, which have historically been well instrumented and well probed, implies that the corresponding coupling must be very weak. Nevertheless, it may remain possible to skirt existing bounds while strongly enhancing the electron recoil at very low energies. For example, with  $E_\nu = 2$  MeV,  $M_{Z'} = 1$  keV, and  $g_{\nu,Z'}g_{e,Z'} = 10^{-13}$ , the new physics rate from electron scattering on a germanium target always exceeds the new rate from nuclear scattering, drops below the SM rate above 10 keV, and sharply exceeds the SM nuclear coherent scattering rate below about 15 eV, recovering the advantage of bandwidth compression conventionally held by the nuclear recoil. Moreover, this contribution may still be disentangled from the standard SM coherent nuclear scattering signal via identification of the characteristic  $E_R^2$  power law enhancement shape.

Interestingly, the electron recoil differential cross section can grow more rapidly (in a logarithmic sense) with increasing coupling than the nuclear recoil at low energies. The reason for this is that the new physics contribution will include both a cross term with the SM, and a square of the new physics amplitude, and the SM contribution is already large for the nuclear scattering case. When the new physics amplitude is smaller than the SM amplitude, the scaling with BSM couplings will be linear, but when the new physics amplitude is larger, the scaling with BSM couplings is quadratic.

The possibility of a scalar or pseudoscalar mediator  $\phi$  has several clear distinctions from that of a neutral vector mediator. Most essentially, a scalar coupling to two spinors mixes

left and right chiralities, as would a mass term, whereas the vector mediator necessitates the insertion of a vector of gamma matrices between the spinors, which will not mix chirality. If it exists, the right-handed neutrino chirality has no standard model interactions. Indeed, the solar or reactor source will consist of solely left-handed neutrinos (or right-handed anti-neutrinos). However, the described experimental construction is insensitive to the nature of the exiting neutrino, and there is no direct prohibition against a sterile neutrino playing this role. More importantly, however, given that the SM has no process with identical initial and final states, there will be no SM interference terms generated (again, these are not necessarily vital to prospects for detection). Additionally, the scalar and pseudoscalar scenarios are prohibited from mixing, such that only the squares of individual couplings are referenced in the differential cross section. This has the additional interesting consequence that neutrino and anti-neutrino scattering are equivalent, and insensitive to relative inversions of phase. Additionally, incompatibility of the Lorentz structure implies that it is impossible in this case to tidily summarize the new physics as a shift in the couplings of the neutral current SM vector boson exchange. The full additions to Eq. (1), for a single particle with couplings  $[g_{X,S}, g_{X,PS}] \equiv g_{X,\phi} \times [\cos \alpha_\phi, \sin \alpha_\phi]$  to the field  $\phi$ , are as follows.

$$\frac{d\sigma}{dE_R} \supset \frac{g_{\nu,\phi}^2 g_{X,\phi}^2 (E_R^2 m_X + 2E_R m_X^2 \cos \alpha_\phi)}{8\pi E_\nu^2 (2E_R m_X + M_\phi^2)^2} \quad (9)$$

In Fig.1 we have plotted example recoil spectra for  $\bar{\nu}_e$ -nucleus and  $\bar{\nu}_e - e^-$  scattering in germanium and silicon detectors. These spectra highlight several important points: i) the motivation for low threshold detectors is obvious from the rise in the spectrum at low recoil energies, ii) the new interactions can produce deviations from the SM that could be within reach for near term experiments, and iii) the interference between the pure SM interaction and the SM plus simplified model interactions may produce destructive interference effects from  $V$  and  $AV$  exchange.

#### IV. ULTRA-LOW THRESHOLD DETECTORS WITH REACTOR NEUTRINOS

In order to calculate the rate of recoil for nuclei we must specify the flux and energy distribution of incident neutrinos. Here we primarily consider reactor neutrinos, detected via CE $\nu$ NS using ultra-low threshold detectors. However, for comparison of sensitivity we will also consider Solar neutrinos and stopped pion sources. These flux components are

TABLE I. Neutrino flux sources and their respective uncertainties in the flux normalizations. The SNS flux and uncertainty was taken from [20]. The Solar components are derived from the high metallicity Solar model as outlined in Ref. [38].

component	$\nu$ flux ( $\text{cm}^{-2}\text{s}^{-1}$ )
TAMU reactor (at 1m)	$1.50(1 \pm 0.02) \times 10^{12}$
SNS (at 20m)	
$\nu_\mu$ (prompt)	$4.30(1 \pm 0.1) \times 10^7$
$\nu_e$ (delayed)	$4.30(1 \pm 0.1) \times 10^7$
$\bar{\nu}_\mu$ (delayed)	$4.30(1 \pm 0.1) \times 10^7$
Solar	
pp	$5.98(1 \pm 0.006) \times 10^{10}$
${}^7\text{Be}$	$5.00(1 \pm 0.07) \times 10^9$
${}^8\text{B}$	$5.58(1 \pm 0.14) \times 10^6$
pep	$1.44(1 \pm 0.012) \times 10^8$

summarized in table I.

To investigate the reach of reactor neutrino sources in probing NSI with light mediators, we consider the Mitchell Institute Neutrino Experiment at a Reactor (MINER). As a brief review, the MINER program has been developed with the Nuclear Science Center at Texas A&M University (TAMU), which administrates a megawatt-class TRIGA-type pool reactor stocked with low enriched ( $\sim 20\%$ )  ${}^{235}\text{U}$ . Low temperature solid state germanium and silicon detectors, using technology similar to that currently developed for direct dark matter searches like SuperCDMS, will be installed at very near proximity ( $\sim 1 - 3\text{m}$ ) to the reactor core. More specifics on the reactor, its properties, and the MINER program may be found in recent works which have highlighted its physics potential for TeV scale mass  $Z'$  models, sensitivity for neutrino magnetic moment searches, and sterile neutrino searches [10, 11].

The antineutrino flux can be obtained via knowledge of the reactor's power ( $1.00 \pm 0.02$  MW in the present work) along with the normalized antineutrino fission spectrum, which has been measured at various sites (for a recent discussion of the current status of the spectrum see [39]). The spectrum has not been directly measured below the 1.8 MeV inverse beta decay threshold. For these energies we adopt the theoretical distribution in Ref. [40]. Above

1.8 MeV we use the experimental results of Ref. [41].

We assume a detector exposure corresponding to germanium and silicon masses each of 10kg, together with a five year running time, as is realistic for the MINER experiment. As previously mentioned, an extremely important aspect of the detector technology is the existence of low thresholds for nuclear recoils (nr), due to the expected features in CE $\nu$ NS that arise at recoil energies below the keV scale. We assume a 100eVnr threshold for germanium and silicon. While no current technology exists that reaches such thresholds, experimental progress is underway which can conceivably reach these levels in the near future [42]. For example, CDMSlite recently achieved a threshold of 56eVee (electron recoil) [37] and a few hundred eVnr (the exact conversion factor from eVee to eVnr depends on the parameterization for the ionization yield, which is only known to within a factor of a few). The proximity to the reactor, while ensuring a large neutrino flux, comes with a commensurately large neutron and gamma background. The goal for the MINER experiment is approximately 100 events per day per kg per keV, i.e. 100 dru, in the signal region. Modeling of the reactor, detector and shielding show that this goal should be achievable [43], and thus we will use a flat background of 100dru as a baseline. These detector specifications are summarized in table II. In addition, we include a more optimistic future scenario (Ge/Si II), to show the improvement that detector technology developments could yield.

TABLE II. Detector specifications

Name	Target	Exposure (kg.days)	$E_{th}$ (eV)	background (dru)
Ge	germanium	10,000	100	100 $\pm$ 10
Ge II	germanium	10,000	10	10 $\pm$ 1
Ge II(low BG)	germanium	10,000	10	(1 $\pm$ .1) $\times$ 10 <sup>-4</sup>
Si	silicon	10,000	100	100 $\pm$ 10
Si II	silicon	10,000	20	10 $\pm$ 1
CsI	Caesium-Iodide	10,000	5,000	10 $\pm$ 1

The distribution of solar neutrinos presents either large flux at low energies, or low flux at large energies, as in table I. The highest flux rates are from the pp process, integrating to approximately  $6 \times 10^{10} \text{ cm}^{-2}\text{s}^{-1}$  and cutting off around 0.4 MeV, followed by the <sup>7</sup>Be and pep line sources at 0.9 and 1.4 MeV with corresponding fluxes  $5 \times 10^9$  and  $1 \times 10^8 \text{ cm}^{-2}\text{s}^{-1}$

(largely dominant over the N, O, F continuum), and the broad  $^8\text{B}$  source that extends out to more than 15 MeV with an integrated flux of  $6 \times 10^6 \text{ cm}^{-2}\text{s}^{-1}$ . In order to access the CE $\nu$ NS process with near-term detector technology, it is necessary that the neutrino source have an energy in the few MeV range. For example, a nuclear recoil detector threshold around (20, 10) eV is required in (silicon, germanium) in order to register about half of the scattering events from neutrinos with a mean energy of 1.5 MeV [10]. The threshold scales as a square with  $E_\nu$ , such that  $E_\nu = 0.5 \text{ MeV}$  would require sensitivity at the level of about (5, 2.5) eV, approaching the theoretical limit for single electron ionization resolution [42]. Electron recoils require no such dramatic sensitivity, but they generally suffer with respect to rate and diffuse background contamination for the reasons described previously. For the spectral components where CE $\nu$ NS could be presently visible, the flux is woefully low. By comparison, a nuclear reactor presents an (electron antineutrino) spectral composition distributed across the few MeV range that can exceed all of the solar flux by orders of magnitude, typically  $10^{12-13} \text{ cm}^{-2}\text{s}^{-1}$  [10, 44, 45]. This combination presents obvious advantages for the rate of signal events, although it likewise presents new challenges with respect to the management of radiologically intense backgrounds [43].

In addition to neutrinos from reactor and solar sources, stopped pion sources, such as at the SNS, produce neutrinos through the decay of muons at rest. These sources present the lowest fluxes, but at a much higher energy with a well known flux. The higher energy allows the use of more conventional detectors with modest thresholds of a few keV, such as the CsI detectors employed in the first phase of the COHERENT experiment [20].

## V. COMPUTATION OF CONFIDENCE INTERVALS AND LIMITS

Before competitive limits can be placed on new physics, the standard model CE $\nu$ NS process must be discovered and measured. The MINER experiment can expect  $\sim 10$  dru from SM CE $\nu$ NS, providing a signal-to-noise ratio of 1:10. From this we estimate that a  $5\sigma$  signal will be observed with a few months of run-time. To quantify how well the CE $\nu$ NS cross section can be measured we will use the profile likelihood test statistic:

$$t_\mu = -2\log \frac{\mathcal{L}(\mu, \hat{\theta})}{\mathcal{L}(\hat{\mu}, \hat{\theta})}, \quad (10)$$

where  $\mu$  is the signal strength,  $\frac{\sigma}{\sigma_{\text{SM}}}$ , and  $\theta$  represents the nuisance parameters. Hatted parameters denote a maximization. We will use a binned likelihood function given by:

$$\mathcal{L} = \prod_i \frac{\nu_i^{n_i} e^{-\nu_i}}{n_i!} \prod_j e^{-\frac{1}{2\delta_j^2}(1-N_j)^2}. \quad (11)$$

Here  $\nu_i$  and  $n_i$  are the expected (SM) and observed events in each bin, and the second product is a Gaussian likelihood summed over the nuisance parameters: the background and flux component normalizations  $N_j$  (one, three and four components for the reactor, SNS and solar cases respectively, where the values are given in table I). The test statistic is then used to derive the expected 90% confidence intervals on the signal strength using the Asimov dataset [46]. Fig. 2 shows the confidence intervals and discovery significance as a function of exposure for several example experiments. The MINER experiment (situated at 2m from the reactor) will be able to discover the SM process within 100kg-days and constrain the SM cross section to  $\pm 10\%$  with  $10^3$ kg-days of exposure, even with the conservative background and threshold assumptions. The solar and SNS neutrino experiments require roughly 100 times as much exposure to achieve the same discovery potential and measurement accuracy. This is due to the smaller fluxes and larger uncertainties in these experiments.

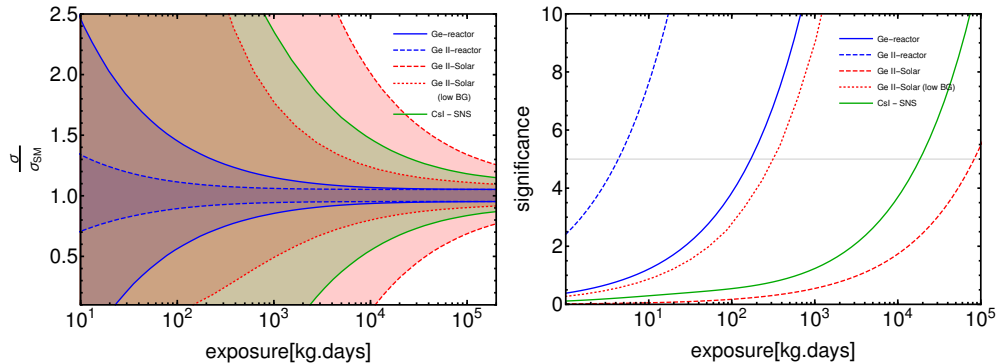


FIG. 2. *Left*: 90% confidence intervals on the standard model CE $\nu$ NS cross section from a selection of experiments. *Right*: exposure required to reach a 5- $\sigma$  fluctuation from the background only hypothesis.

To investigate the experimental reach of the MINER experiment we calculate discovery limits for the detector configurations listed in table II, based on the flux of the TAMU reactor at 2m. The limits are also calculated for the same detectors with Solar neutrinos as the source. For comparison with a current experiment we have also included the discovery limits

for the first phase of the COHERENT experiment. The various neutrino sources cannot be distinguished by the detector, and thus the reactor and SNS cases should thus include the solar neutrinos as well, although the limits are displayed separately for illustration. Given that a dedicated solar experiment would likely be carried out deep underground (not in close proximity to a nuclear reactor), we have also included the calculation for a Ge II experiment in a background-free environment. The discovery limits are defined as the smallest signal that could produce a  $3\sigma$  fluctuation 90% of the time. To find this limit we use a binned likelihood function, Eq. 11 with log-spaced bins. The likelihood is used to calculate the log-likelihood ratio and generate the test statistic  $q_0$ , from which we may estimate the expected median significance of an experiment via the Asimov dataset [46].

$$q_0 = \begin{cases} -2\log\frac{\mathcal{L}(\mu=0,\hat{\theta})}{\mathcal{L}(\hat{\mu},\hat{\theta})} & \sigma \geq \hat{\sigma} \\ 0 & \sigma < \hat{\sigma} \end{cases} \quad (12)$$

## VI. DISCOVERY LIMIT RESULTS

The discovery limits for each of the four BSM models are shown in figure 3. For nuclear scattering, the parameters  $f_n$ ,  $b_n$  and  $a_0$  shown in the plots are respectively the scalar, vector, and axial vector analogs of the electron scattering coupling product ( $g_{\nu,Z'} g_{e,Z'}$ ), but at the per nucleon or per unit spin level. We assume no isospin violation, such that the corresponding coherency factors for the nucleus at large are simply ( $Q'_s = f_n A$ ), ( $Q'_v = b_n A$ ), and ( $Q'_a = a_0 \langle S \rangle$ ). A first glance through each of the Fig. 3 plots will reveal an essentially similar “hockey stick” curve profile, the general shape of which can be understood in terms of the momentum transfer.

As the mediator mass is decreased, the cross section increases, and thus the experiments are sensitive to smaller values of the couplings. For heavier mediator masses, the coupling (or rather the product of mediator couplings to the neutrino and to the scattering target) sensitivity is diminished with a log-log slope of 2, due to effects of the new physics interaction and propagator in the large-mass (point-like interaction) regime, where one has a Fermi styled contribution  $g_{\nu,Z'} g_{X,Z'} / M_{Z'}^2$ . This ratio is constant along the ( $\log g_{\nu,Z'} g_{X,Z'} = 2 \log M_{Z'}$ ) line. Conversely, the mediator mass may be neglected when it becomes small compared to the momentum transfer. The relevant term here is  $g_{\nu,Z'} g_{X,Z'} / 2E_R m_X$ , which corresponds

to a flat coupling limit sensitivity. There is a transition regime that interpolates between these two asymptotes, wherein the coupling sensitivity bends smoothly. Looking again at the propagator, we can infer that this knee in the sensitivity should be centered around  $M_{Z'} \simeq \sqrt{2E_R m_X}$ . This knee occurs at a lower mediator mass for electron scattering since the momentum transfer is much smaller in that case. Limiting momentarily to the dominant vector interaction of Eq. (1), and factoring out couplings and constant terms, the functional dependence of the differential cross-section may be very well approximated as a linearly declining function of  $E_R$  that cuts off at  $E_R^{\max}$ , as specified in Eq. (8).

$$\frac{d\sigma}{dE_R} \simeq 1 - \frac{E_R}{E_R^{\max}} \quad (13)$$

It should be understood that the light vector mediator and scalar mediator interactions imply complications to this simplified structure, as in Eq. (7) and Eq. (9) respectively, although certain universalities persist. For a detector sensitivity threshold  $E_R^{\min}$ , and considering a monochromatic neutrino source energy  $E_\nu$ , the integrated area under this curve is  $(E_R^{\max} - E_R^{\min})^2/2E_R^{\max}$ , or simply  $E_R^{\max}/2$  if the threshold ( $E_R^{\min} \ll E_R^{\max}$ ) is much smaller than the cutoff. Likewise, the mean recoil is  $\langle E_R \rangle = (2E_R^{\min} + E_R^{\max})/3$ , and the standard deviation of the recoil is  $\sigma_{E_R} = (E_R^{\max} - E_R^{\min})/3\sqrt{2}$ . This suggests that the sensitivity knee for nuclear recoils should be centered around  $E_\nu$ , or around the geometric mean  $\sqrt{m_e E_\nu}$  for electron recoils. The propagated width in the mediator mass is  $\sigma_{M_{Z'}} = \sqrt{m_X/2\langle E_R \rangle} \times \sigma_{E_R}$ , which implies a fractional width  $\sigma_{M_{Z'}/M_{Z'}} \simeq 1/2\sqrt{2}$  that is independent of  $m_X$  at leading order. However, for scattering that is widely spread across a continuum of source energies  $E_\nu$ , the width will be additionally correspondingly broadened.

We may test the prior conclusions against the numerical results in Fig. 3. For germanium, the minimal neutrino energy that can create a recorded recoil (for head-on collisions, which have the lowest cross section) is around 0.5 or 2 MeV, for threshold sensitivities  $E_R^{\min}$  of 10 or 100 eV, respectively. Conversely, electron recoils can be sensitive to neutrinos as soft as a few keV. In the nuclear recoil column, we observe a rather sharp transition knee, centered at around 1 or 4 MeV for the baseline and future threshold scenarios, which is stable across the different simplified models. As expected, each is a bit larger (about a factor of two) than the kinematic turn-on. By eye the full width of the transition region is approximately one order of magnitude in mass. This suggests, consistently, that the continuum nature of the solar and reactor sources is relevant here. Looking at the electron scattering columns, we should expect



a substantially wider transition region, which starts at much lower masses, because the lower reaches of the applicable neutrino energy spectra are not kinematically eclipsed. We should observe, furthermore, that there is a less appreciable leftward shift in the position of the knee for the second generation threshold sensitivity since most relevant electron scattering events are already integrated at very modest values of  $E_R^{\min}$ . Based simply on the very wide range of electron recoil energies  $E_R$  which are sampled, spanning from threshold near 100 eV up to more than 10 MeV, we can expect a transition region around the knee in  $M_{Z'}$  that may cover more than two orders of magnitude, from approximately 10 keV, up to a few MeV. We additionally observe more variation in the exact position and width of the knee between the four BSM models in the electron scattering case.

In Fig. 3, we plot the plateau sensitivity in the low mediator mass limit as a function of the experimental recoil threshold. As expected, going a lower threshold benefits the reach of the experiments, especially in the low mediator mass region. This effect is more pronounced for nuclear scattering since the electron scattering rate is flat with energy. The limiting factor of sensitivity to electron scattering is the background (which is also flat), when it is removed the sensitivity increases more than for nuclear scattering. The nuclear recoil plots clearly exhibit a staircase behavior in sensitivity for the Solar sources, as the  ${}^7\text{Be}$  and pep line sources turn on at lower detection thresholds. Comparing individual experiments for a given BSM scenario, the larger flux of a reactor experiment allows for a greater reach when compared to an equivalent solar experiment. However, this gap is smaller when considering electron scattering, since the pp rate is able to contribute throughout the signal region, whereas for nuclei scattering the pp rate is below the detector threshold. Additionally, comparing with a solar experiment performed in a background free environment, we find that the reactor experiments will still have a greater reach in most BSM scenarios explored. These conclusions are the same for the silicon experiments, the plots of which we have included in the appendix. In the proposed configuration the silicon detectors are under-powered compared to germanium, owing to the smaller detector mass and fewer neutrons per nuclei. The utility of the silicon component of the experiment is in confirming a putative signal, not in adding statistical power to the overall sensitivity. Having two detector materials would also provide complementary information in the event of a discovery, for example, if there is isospin violation.

To compare the reach of a reactor experiment with a more general set of constraints we

examine a  $U(1)_{\text{B-L}}$  model with a light vector mediator of mass  $m_{Z'}$  with coupling  $g_{\text{B-L}}$  described by the Lagrangian

$$\mathcal{L}_{\text{B-L}} \supset g_{\text{B-L}} Z'_\mu \left( \frac{1}{3} \bar{q} \gamma^\mu q - \bar{\nu} \gamma^\mu \nu - \bar{e} \gamma^\mu e \right) \quad (14)$$

This model has also been explored for CE $\nu$ NS sourced by solar neutrinos with G2 and future direct detection experiments [27, 28]. Fig.6 shows the reach in the  $g_{\text{B-L}} - m_{Z'}$  space for the MINER scenario outlined above. The thick solid red curve gives the reach due to nuclear scattering, and the thick solid blue curve is the reach for electron scattering.

A few aspects of this plot are worth detailing. First, this demonstrates that a reactor experiment employing low threshold detectors such as planned for MINER can provide world leading constraints in large regions of parameter space. Interestingly we find that the nuclear scattering constraints are greater than those from electron scattering, which is a novel feature of the reactor experiment. Additionally, the reach for nuclear scattering from the reactor is well below the reach for nuclear scattering from solar neutrinos. The blue and gray shaded regions are constraints from other experiments, whose details can be found for example in [27, 28].

## VII. SCALING RULES

In Sec. III, we intuitively characterized the shape and scale of contributions to the differential cross section for electron and nuclear scattering from the exchange of a new light mediator. In Secs. V and VI, we outlined the statistical machinery by which these profiles for new physics may be leveraged to set discovery limits, and plotted limit curves in the coupling vs. mass plane for various assumptions of the mediator spin, coupling type, background control, and detector sensitivity. In the present section, we deconstruct this analysis approximately, but in closed form, in order to develop an intuitive predictive framework for assessing experimental sensitivity.

In particular, we consider the asymptotic coupling sensitivity in the massless mediator limit ( $m_{Z'}^2 \ll 2E_R m_X$ ), and attempt to establish rules for the relative scaling of this limit with respect to variations such as the detector threshold  $E_R^{\text{min}}$ , the neutrino source (solar or reactor) and energy  $E_\nu$ , the target mass (either an electron or a nucleus), and the various BSM simplified models. In particular, we will attempt to develop a framework whereby

one may approximately infer a family of related discovery limits from knowledge of any one member. In order to understand these relative sensitivities, it is essential to inspect the way that the discovery limit is calculated, in terms of the log-likelihood ratio  $q_0$  defined in Eq. (12). After canceling the background contributions, and the nuisance parameter terms (neglecting subleading model dependencies in their optimization), we observe that any two models  $A$  and  $B$  will induce the same statistical deviation  $\Delta q_0$  from the SM if  $\log \mathcal{L}_A = \log \mathcal{L}_B$ . Since all discovery limits will correspond to achieving a  $\Delta q_0$  equal to certain Asimov number, we can use this condition to solve for the desired scaling factors.

For simplicity, we will reduce the binned likelihood in Eq. (11) to a single integration. Additionally, we notice that in the limit of large event counts, the Poisson distribution reduces to the Gaussian with expected number  $\nu$ , observed number  $n$ , and standard deviation  $\sigma = \sqrt{\nu}$ .

$$-2 \log \mathcal{L} = \frac{(n - \nu)^2}{\nu} \quad (15)$$

Note that  $(n - \nu)$  is the unified BSM event rate, including any potential mixing terms with the SM. We will have the same SM background rate  $\nu$  for various models, so the criterion for comparison of limits reduces in this approximation simply to equality of (the absolute value of) the signal event deviation  $|n - \nu|$ , or equivalently to equality of the magnitude of the BSM cross section (allowing also for negative interference).

In order to extract simplified relationships on the new physics couplings  $Q'$ , we need to isolate the leading terms, focusing now specifically on the nuclear scattering example. Given reasonable event rates and reliable background characterization, experiments will be sensitive to small deviations from the SM rate. The largest SM contributions are from the vector interaction, and this will enhance the cross term for BSM vector mediators. We define the coherent SM vector coupling to the nucleus as  $Q_v \equiv -2 \times [Zg_v^p + (A - Z)g_v^n]$ , consistent with Ref. [28]. Correspondingly, we may neglect the square of the new physics term in this case. By contrast, for axial vector interactions, the mixing term with  $Q_v$  is of order  $\mathcal{O}(E_R)$ , and the mixing term proportional to  $Q_a$  is small because  $Q_a \ll Q_v$ . Thus, we may neglect mixing in this case, and take the square of the new physics amplitude to be leading. For the scalar interactions, no cross term with the SM exists. The associated cross-sections are

calculable.

$$n - \nu \approx \int_{E_R^{\min}} dE_R \int_{(E_R + \sqrt{E_R^2 + 2E_R m_N})/2} dE_\nu \frac{f(E_\nu)}{f(E_\nu)} \times \begin{cases} \frac{f_n^2 A^2}{16\pi E_\nu^2 E_R} & \text{scalar} \\ -\frac{b_n A G_F Q_v}{2\sqrt{2}\pi E_R} \left(1 - \frac{E_R}{E_R^{\max}}\right) & \text{vector} \\ \frac{a_0^2 \langle S \rangle^2}{8\pi m_N E_R^2} \left(1 + \frac{E_R}{E_R^{\max}}\right) & \text{axial vector} \end{cases} \quad (16)$$

where  $f(E_\nu)$  is the anti-neutrino flux. For a monochromatic beam, we may integrate in closed form, retaining leading terms.

$$|n - \nu| \approx \begin{cases} f_n^2 \times c_s \equiv \frac{A^2}{16\pi E_\nu^2} \ln\left(\frac{E_R^{\max}}{E_R^{\min}}\right) & \text{scalar} \\ b_n \times c_v \equiv \frac{A G_F Q_v}{2\sqrt{2}\pi} \left[\ln\left(\frac{E_R^{\max}}{E_R^{\min}}\right) - 1\right] & \text{vector} \\ a_0^2 \times c_a \equiv \frac{\langle S \rangle^2}{8\pi m_N E_R^2} & \text{axial vector} \end{cases} \quad (17)$$

For a germanium target, we can take approximately ( $A \rightarrow 73$ ), ( $m_N \rightarrow 68$  GeV), ( $Q_v \rightarrow 38$ ), and ( $\langle S \rangle \rightarrow 0.5$ ), for  $^{73}\text{Ge}$  with isotopic fraction ( $\text{IF}_{73} = 0.08$ ). Also, we have  $G_F = 1.17 \times 10^{-5} \text{ GeV}^{-2}$ . We will use  $E_R^{\min} = 100$  eV, corresponding to the first generation experiment, and select a representative neutrino energy that is large enough to regularly trigger recoils above the threshold, say  $E_\nu = 4$  MeV, which implies  $E_R^{\max} \simeq 470$  eV. We may then estimate the relative limits ( $b_n/f_n^2 \simeq c_s/c_v \rightarrow 5 \times 10^9$ ), and ( $b_n/a_0^2 \simeq c_a \times \text{IF}_{73}/c_v \rightarrow 6 \times 10^4$ ), holding the event rate constant. Taking the calculated reactor flux limit ( $b_n = 10^{-12}$ ) for the vector coupling, we can predict ( $f_n \simeq 1 \times 10^{-11}$ ) and ( $a_0 \simeq 4 \times 10^{-9}$ ) for the corresponding scalar and axial vector limits, which agree very closely with the detailed calculations illustrated in Fig. 3. Holding each of the Eq. (17) integrated rates constant, we can extract slopes for variation of the coupling limits with respect to changes in the threshold  $E_R^{\min}$ .

$$\begin{cases} \frac{d \log f_n}{d \log E_R^{\min}} \simeq \frac{1}{2 \ln(E_R^{\max}/E_R^{\min})} & \text{scalar} \\ \frac{d \log b_n}{d \log E_R^{\min}} \simeq \frac{1}{\ln(E_R^{\max}/E_R^{\min}) - 1} & \text{vector} \\ \frac{d \log a_0}{d \log E_R^{\min}} \simeq \frac{1}{2} & \text{axial vector} \end{cases} \quad (18)$$

A typical value of  $\ln(E_R^{\max}/E_R^{\min})$  is around 2. This suggests that each of the plots in the lefthand column of Fig. 5 should have a log-slope of order approximately one, steepest for the vector case, and trending steeper as one approaches the kinematic cutoff, which is broadly consistent with what is observed in the detailed calculation. The electron scattering plots

are by contrast flat with respect to variation of the threshold. This is not because the rate does not increase at low recoils, but rather because the event rate in this region is typically dominated by nuclear recoils. In order to carry out a corresponding single bin treatment of electron scattering, one would need to select an integration region which begins at a fixed scale around  $E_R^{\min} \simeq 2$  keV, where the CE $\nu$ NS differential cross section tapers off and is eclipsed by the electron rate, as in Fig. 1. A possible exception to this conventional scenario may arise for a sufficiently light mediator, if the electron rate is able to climb steadily in the keV region, to finally compete with the nuclear rate in the exceptionally soft recoil region, as described toward the end of Sec. III.

Next, we will briefly consider the relative strengths of limits achievable with solar and reactor sources in the case of nuclear scattering. Again, the strategy will be to hold the ratio  $(n - \nu)^2/\nu$  constant. We observe that both the BSM signal and SM background will scale linearly with the integrated flux  $\Phi$ , such that the ratio to be held constant is likewise linear in  $\Phi$ . A first generation experiment will be sensitive primarily to the  $^8\text{B}$  continuum, whose net flux is diminished by a factor of  $\mathcal{O}(10^5)$  relative to that of the reactor site under consideration at the bare minimal baseline. Additionally, however, there is sensitivity to the energy of the source, with the event rate scaling as  $E_\nu^2$ . The mean energy of this solar source is a factor of a few larger than that of a terrestrial reactor, which offsets the rate advantage by approximately one order of magnitude, to  $\mathcal{O}(10^4)$ , in the square. The critical ratio  $(n - \nu)^2/\nu$  is finally proportional to  $\Phi \times (f_n^4, b_n^2, a_0^4)$  in the scalar, vector, and axial vector models, after squaring the leading signal contributions from Eq. (17). This suggests that the solar limits should be weaker by about a factor of 100 in the vector case, or about 10 in the scalar and axial cases. This result is complicated by the non-trivial response of each limit to background rates. Indeed, if one compares the first generation solar and reactor limits in Fig. 3, the solar scattering disadvantage is more pronounced than predicted. However, the lower-background second-generation limit ratios are broadly consistent with the simplified expectation. Similarly, as the recoil sensitivity threshold is reduced sufficiently to access the  $^7\text{Be}$  and pep line sources in Fig. 5, one sees discrete improvements in sensitivity consistent with predictions around 5–6 (scalar, axial vector) or 2–3 (vector) corresponding to escalation of the flux by a factor of around 30.

Finally, in the large mediator mass region,  $2m_N E_r \ll m^2$ , we can estimate the order of  $Q'$  by comparing the BSM “charge” to the SM charge:  $\frac{1}{\sqrt{2}G_F} \frac{Q'_v}{m_z^2} = \frac{1}{2}Q_v$ , so  $Q' = \frac{\sqrt{2}}{2}m^2 G_F Q_v$ .

In order to distinguish BSM from SM signal, one should need  $Q'$  larger than this value.

## VIII. CONCLUSION

Coherent elastic neutrino-nucleus scattering is a process with intriguing prospects for testing Standard Model physics and beyond. Though its measurement has been an experimental target for many years, only recently has technological innovations made an observation realistically imminent. With various collaborations such as COHERENT, CONNIE, TEXONO, and MINER currently taking data or planning to take data in the very near future, and with the possibility of using direct dark matter detection to test CE $\nu$ NS through detection of the solar neutrino flux, the time is ripe to determine the extent to which these various experimental avenues can explore new physics.

In the present work we have examined the effect of new, light mediating particles on both the CE $\nu$ NS process as well as electron scattering by neutrinos, by employing a simplified model approach including new scalar, pseudoscalar, vector, and axial-vector mediators with sub-GeV masses. Such low mass mediators can create a substantial enhancement in the rate of CE $\nu$ NS and  $\nu - e$  scattering at low recoil energies, further motivating the continued push towards low threshold detector technology.

Within this simplified model framework we have determined the projected reach of experiments using low-threshold germanium and silicon detectors at a distance of  $\sim 1 - 3\text{m}$  from the core of a MW class nuclear reactor neutrino source (with the proposed MINER experimental configuration serving as a prototype), next generation Ge and Si direct dark matter detection experiments, as well as the currently running CsI detector deployed by the COHERENT group at the SNS at ORNL (the experimental parameters for these setups are given in Table II). Following other recent studies in this area, we have adopted a  $U(1)_{\text{B-L}}$  BSM framework, and found that low-threshold Ge detectors at close proximity to a nuclear reactor have superior prospects for probing this model, as demonstrated in Fig.6. We have also provided scaling rules that bolster our numerical results, which also provide an intuitive guide to the discovery potential of the CE $\nu$ NS and  $\nu - e$  processes in the coupling and mass parameter space when new light mediators are considered.

Experimental groups are poised on the cusp of a first-ever measurement of the CE $\nu$ NS process. Theoretical efforts such as those detailed in the present work, combined with

continued progress on the experimental front offer intriguing possibilities for near term results within this exciting new region of particle physics.

## IX. ACKNOWLEDGEMENTS

We thank Rupak Mahapatra for useful discussions. BD acknowledges support from DOE Grant DE-FG02-13ER42020. LES acknowledges support from NSF grant PHY-1522717. JWW acknowledges support from NSF grant PHY-1521105. JBD and JWW thank the Kavli Institute for Theoretical Physics for generous hospitality, hot coffee, and a most conducive view during the early stages of this work.

- 
- [1] R. Essig et al., in *Proceedings, Community Summer Study 2013: Snowmass on the Mississippi (CSS2013): Minneapolis, MN, USA, July 29-August 6, 2013* (2013), 1311.0029, URL <http://inspirehep.net/record/1263039/files/arXiv:1311.0029.pdf>.
  - [2] D. Z. Freedman, *Phys. Rev.* **D9**, 1389 (1974).
  - [3] L. M. Krauss, *Phys. Lett.* **B269**, 407 (1991).
  - [4] J. Barranco, O. G. Miranda, and T. I. Rashba, *JHEP* **12**, 021 (2005), hep-ph/0508299.
  - [5] J. Barranco, O. G. Miranda, and T. I. Rashba, *Phys. Rev.* **D76**, 073008 (2007), hep-ph/0702175.
  - [6] J. A. Formaggio, E. Figueroa-Feliciano, and A. J. Anderson, *Phys. Rev.* **D85**, 013009 (2012), 1107.3512.
  - [7] P. deNiverville, M. Pospelov, and A. Ritz, *Phys. Rev.* **D92**, 095005 (2015), 1505.07805.
  - [8] T. S. Kosmas, O. G. Miranda, D. K. Papoulias, M. Tortola, and J. W. F. Valle, *Phys. Rev.* **D92**, 013011 (2015), 1505.03202.
  - [9] T. S. Kosmas, O. G. Miranda, D. K. Papoulias, M. Tortola, and J. W. F. Valle, *Phys. Lett.* **B750**, 459 (2015), 1506.08377.
  - [10] B. Dutta, R. Mahapatra, L. E. Strigari, and J. W. Walker, *Phys. Rev.* **D93**, 013015 (2016), 1508.07981.
  - [11] B. Dutta, Y. Gao, R. Mahapatra, N. Mirabolfathi, L. E. Strigari, and J. W. Walker (2015), 1511.02834.

- [12] M. Lindner, W. Rodejohann, and X.-J. Xu (2016), 1612.04150.
- [13] J. R. Wilson, Phys. Rev. Lett. **32**, 849 (1974).
- [14] M. Prakash, J. M. Lattimer, J. A. Pons, A. W. Steiner, and S. Reddy, Lect. Notes Phys. **578**, 364 (2001), [,364(2000)], astro-ph/0012136.
- [15] C. J. Horowitz, K. J. Coakley, and D. N. McKinsey, Phys. Rev. **D68**, 023005 (2003), astro-ph/0302071.
- [16] A. Burrows, S. Reddy, and T. A. Thompson, Nucl. Phys. **A777**, 356 (2006), astro-ph/0404432.
- [17] H.-T. Janka, K. Langanke, A. Marek, G. Martinez-Pinedo, and B. Mueller, Phys. Rept. **442**, 38 (2007), astro-ph/0612072.
- [18] A. Drukier and L. Stodolsky, Phys. Rev. **D30**, 2295 (1984), [,395(1984)].
- [19] B. Cabrera, L. M. Krauss, and F. Wilczek, Phys. Rev. Lett. **55**, 25 (1985).
- [20] D. Akimov et al. (COHERENT) (2015), 1509.08702.
- [21] A. Aguilar-Arevalo et al. (CONNIE), J. Phys. Conf. Ser. **761**, 012057 (2016), 1608.01565.
- [22] H. Bin Li (TEXONO), J. Phys. Conf. Ser. **718**, 062036 (2016).
- [23] J. Billard, L. Strigari, and E. Figueroa-Feliciano, Phys. Rev. **D89**, 023524 (2014), 1307.5458.
- [24] F. Ruppin, J. Billard, E. Figueroa-Feliciano, and L. Strigari, Phys. Rev. **D90**, 083510 (2014), 1408.3581.
- [25] J. B. Dent, B. Dutta, J. L. Newstead, and L. E. Strigari, Phys. Rev. **D93**, 075018 (2016), 1602.05300.
- [26] J. B. Dent, B. Dutta, J. L. Newstead, and L. E. Strigari (2016), 1607.01468.
- [27] R. Harnik, J. Kopp, and P. A. N. Machado, JCAP **1207**, 026 (2012), 1202.6073.
- [28] D. G. Cerdeño, M. Fairbairn, T. Jubb, P. A. N. Machado, A. C. Vincent, and C. Boehm, JHEP **05**, 118 (2016), 1604.01025.
- [29] M. Cirelli, E. Del Nobile, and P. Panci, JCAP **1310**, 019 (2013), 1307.5955.
- [30] P. Agrawal, Z. Chacko, C. Kilic, and R. K. Mishra (2010), 1003.1912.
- [31] K. R. Dienes, J. Kumar, B. Thomas, and D. Yaylali, Phys. Rev. **D90**, 015012 (2014), 1312.7772.
- [32] R. J. Hill and M. P. Solon, Phys. Rev. **D91**, 043505 (2015), 1409.8290.
- [33] S. G. Porsev, K. Beloy, and A. Derevianko, Phys. Rev. Lett. **102**, 181601 (2009), 0902.0335.
- [34] B. C. Canas, E. A. Garces, O. G. Miranda, M. Tortola, and J. W. F. Valle (2016), 1608.02671.
- [35] J. Erler and M. J. Ramsey-Musolf, Phys. Rev. **D72**, 073003 (2005), hep-ph/0409169.



- [36] P. Klos, J. Menéndez, D. Gazit, and A. Schwenk, Phys. Rev. **D88**, 083516 (2013), [Erratum: Phys. Rev.D89,no.2,029901(2014)], 1304.7684.
- [37] R. Agnese et al. (SuperCDMS), Phys. Rev. Lett. **116**, 071301 (2016), 1509.02448.
- [38] W. C. Haxton, R. G. Hamish Robertson, and A. M. Serenelli, Ann. Rev. Astron. Astrophys. **51**, 21 (2013), 1208.5723.
- [39] F. P. An et al. (Daya Bay) (2016), 1607.05378.
- [40] V. I. Kopeikin, Phys. Atom. Nucl. **75**, 143 (2012), [Yad. Fiz.75N2,165(2012)].
- [41] K. Schreckenbach, G. Colvin, W. Gelletly, and F. Von Feilitzsch, Phys. Lett. **B160**, 325 (1985).
- [42] N. Mirabolfathi, H. R. Harris, R. Mahapatra, K. Sundqvist, A. Jastram, B. Serfass, D. Faiez, and B. Sadoulet (2015), 1510.00999.
- [43] G. Agnolet et al. (MINER) (2016), 1609.02066.
- [44] V. Singh and H. T. Wong (TEXONO), PoS **AHEP2003**, 053 (2003), nucl-ex/0412057.
- [45] H. T. Wong, H.-B. Li, J. Li, Q. Yue, and Z.-Y. Zhou, J. Phys. Conf. Ser. **39**, 266 (2006), hep-ex/0511001.
- [46] G. Cowan, K. Cranmer, E. Gross, and O. Vitells, Eur. Phys. J. **C71**, 1554 (2011), [Erratum: Eur. Phys. J.C73,2501(2013)], 1007.1727.

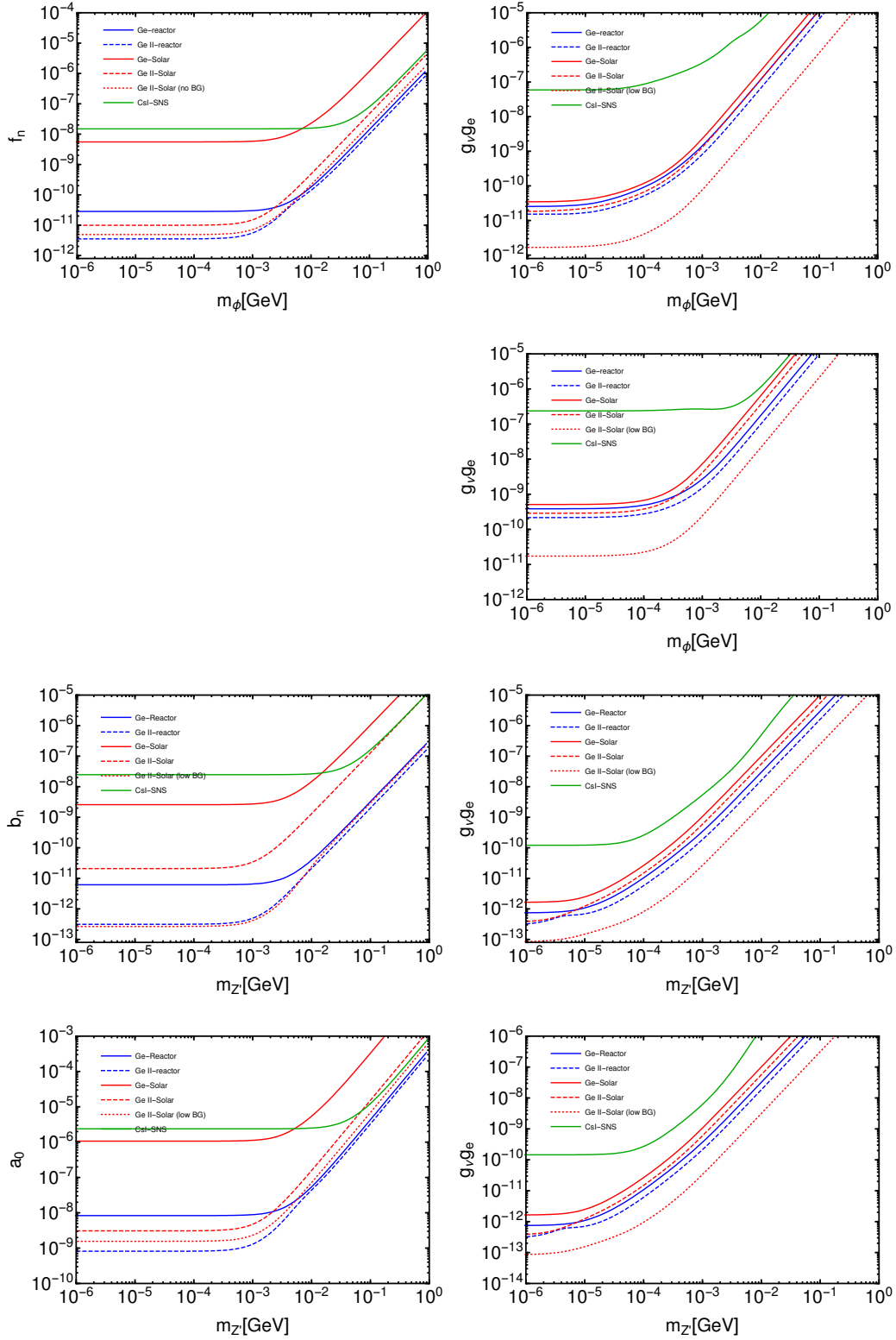


FIG. 3. Discovery limits for neutrino scattering off germanium nuclei (left) and electrons (right), for the different BSM models (from top to bottom): scalar, pseudo-scalar, vector and axial-vector

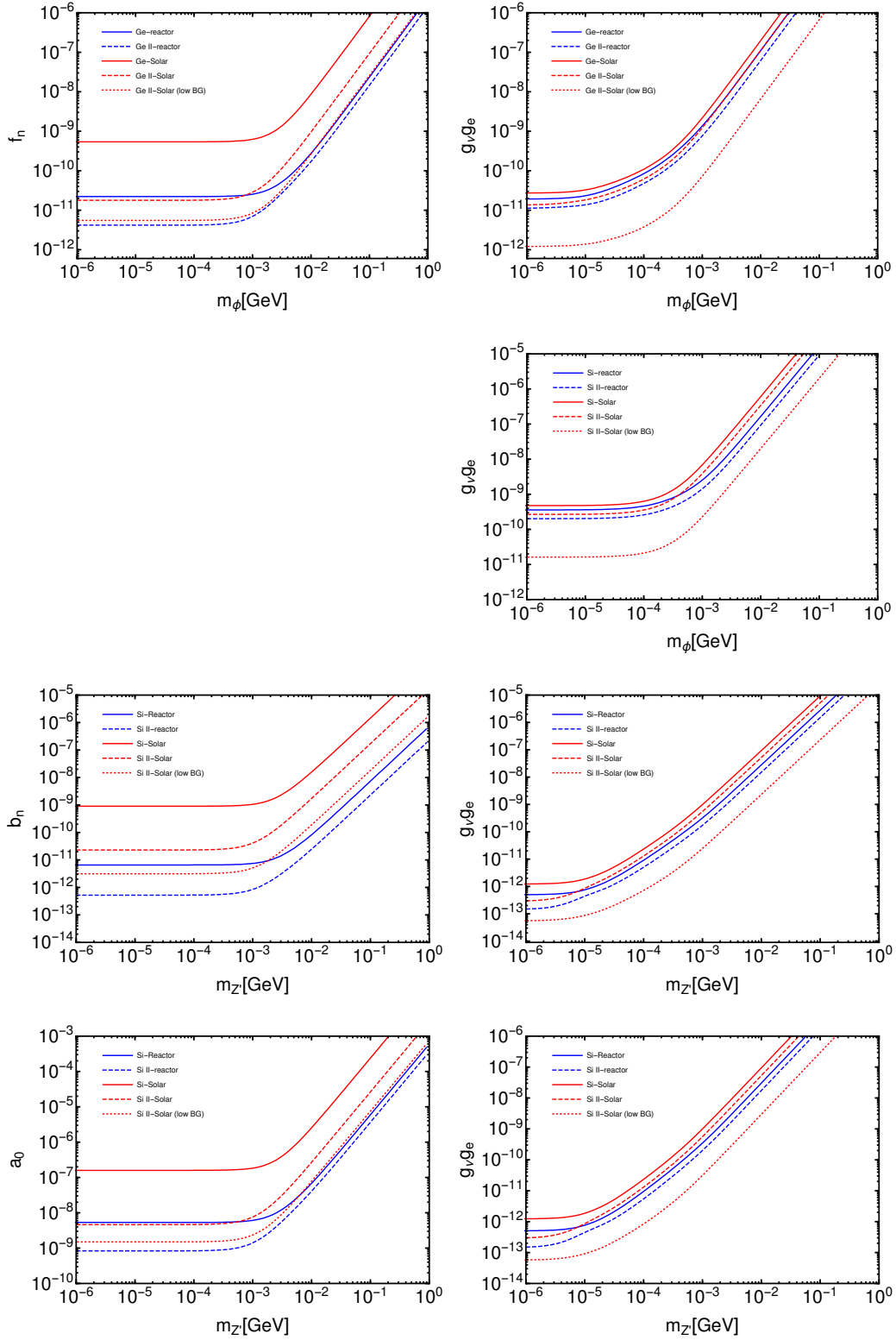


FIG. 4. The same as Fig. 3 but for silicon detectors

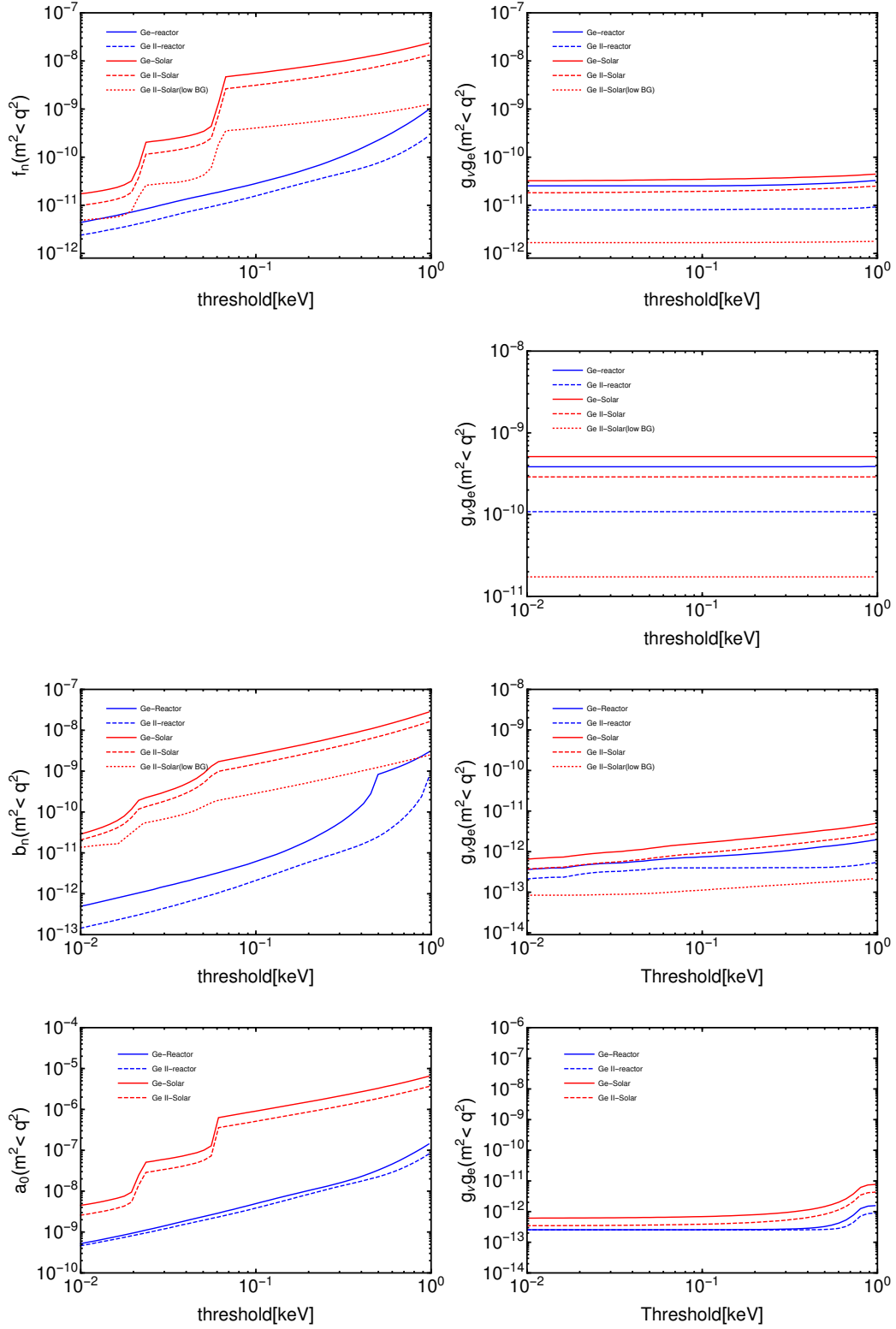


FIG. 5. Discovery limits vs. threshold for neutrino scattering off germanium nuclei (left) and electrons (right), for the different BSM models (from top to bottom): scalar, pseudo-scalar, vector and axial-vector

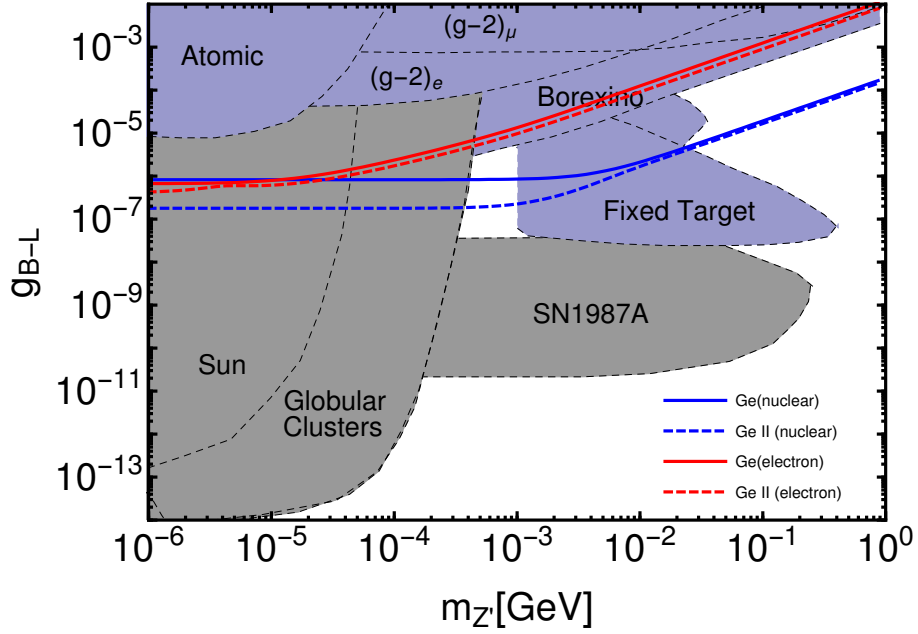


FIG. 6. Predicted exclusion curves in the coupling-mediator mass parameter space in a  $U(1)_{B-L}$  model for electron (red) and nuclear (blue) recoils observed by germanium detectors (phase I and II are solid and dashed respectively) with a total exposure of 10t-days, thresholds situated 2m from a  $\bar{\nu}_e$  flux sourced by a 1MW reactor. The shaded regions are exclusion curves from other experiments and observations, compilation from [27].